Volume 27
Number 14
14 April 2025
Pages 2035–2242

CrystEngComm

rsc.li/crystengcomm

ISSN 1466-8033

ROYAL SOCIETY OF CHEMISTRY

COMMUNICATION

Akiko Hori *et al.*

Yellow and red polymorphic co-crystals of phenyl-substituted pyrazinacene and naphthalene *via* π-hole···π interactions

CrystEngComm

ROYAL SOCIETY OF CHEMISTRY

COMMUNICATION

View Article Online
View Journal | View Issue

Cite this: *CrystEngComm*, 2025, **27**, 2064

Received 30th January 2025,
Accepted 4th March 2025

DOI: 10.1039/d5ce00114e

rsc.li/crystengcomm

Yellow and red polymorphic co-crystals of phenyl-substituted pyrazinacene and naphthalene *via* π-hole···π interactions†

Kazushi Nakada, Gary J. Richards and Akiko Hori *

The phenyl-substituted dicyanoazanaphthalene (1, $C_{20}H_{10}N_6$) is a yellow compound that forms both yellow and red crystals upon co-crystallization with naphthalene (2). These crystals represent a rare example of the polymorphism of 1·2, forming two stable states, elucidating the role of donor–acceptor and π-hole···π interactions in the co-crystallization process. The yellow columnar crystal features an alternating arrangement of 1 and 2, while the red plate crystal exhibits paired 1 and 2 units arranged in a herringbone motif. Although no significant differences in molecular structures were observed, the red crystal, at 160 K, exhibited a higher density (D_c = 1.332 g cm^{-3}) and planarity of the pyrazinacene framework compared to the yellow crystal (D_c = 1.294 g cm^{-3}), which correlates with its distinct optical and luminescent behaviors.

Polymorphism, particularly when studied in combination with color changes associated with structural transformations, has been a widely investigated topic in the field of crystal engineering. Previous studies have primarily focused on single-component crystalline systems, where differences in molecular conformations lead to variations in color.[1–3] For instance, *cis*-platinum complexes are well-known to exhibit polymorphic forms in yellow and red depending on solvent or thermal conditions.[4,5] Structural analyses have revealed that the yellow form corresponds to a longer Pt–Pt distance, while the red form is associated with shorter Pt–Pt distances and the emergence of metal–metal interactions (MMLCT).[6–8] Similarly, Thamattoor *et al.* demonstrated that derivatives of anthracene linked through acetylene bonds form polymorphs that exhibit yellow or red colors.[9] The yellow polymorph corresponds to a planar molecular conformation with a dihedral angle near 90°, whereas the red polymorph is attributed to a non-planar conformation with a dihedral angle close to 0°, highlighting the color switching induced by the π-conjugated system.[10–13] These studies highlight the impact of molecular stereochemistry on crystal packing, a phenomenon of significant interest across diverse fields, including material science and pharmaceuticals.[14–20]

In contrast to single-component systems, the exploration of polymorphism in co-crystals remains underdeveloped.[21–24] Co-crystals, composed of two or more molecular components in fixed stoichiometric ratios, rely on intermolecular interactions such as host–guest or donor–acceptor relationships. Consequently, changes in the primary molecular structure can directly affect guest molecule interactions, leading to either failed co-crystal formation or the emergence of pseudo-polymorphs with varying numbers of guest molecules,[25–28] as often observed in such systems. Here, we report two distinct polymorphs of 1 : 1 co-crystals composed of a pyrazinacene derivative (**1**)[29] and naphthalene (**2**), as shown in Scheme 1. These polymorphs exhibit different colors: a slightly orange-tinted yellow prismatic (**Y**) and a red plate (**R**). Given that the polymorphs share the same stoichiometric composition, we propose that the co-crystal formation involves the preorganization of the host and guest molecules into donor–acceptor pairs, which then stabilize two distinct packing structures. This hypothesis is supported by X-ray crystallographic analyses, which reveal no significant molecular structural differences between the two polymorphs. Thus, the observed color differences cannot be attributed to conventional changes in molecular

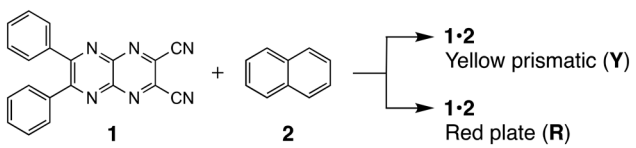

Scheme 1 Molecular structures of **1** and **2**, and the corresponding co-crystals, **1·2**.

Graduate School of Engineering and Science, Shibaura Institute of Technology, Fukasaku 307, Minuma-ku, Saitama 337-8570, Japan.
E-mail: ahori@shibaura-it.ac.jp; Fax: +81 48 687 5013; Tel: +81 48 720 6350

† Electronic supplementary information (ESI) available: TG, crystallographic, and theoretical studies of polymorphs **1·2** were summarized. CCDC 2419629 and 2419630. For ESI and crystallographic data in CIF or other electronic format see DOI: https://doi.org/10.1039/d5ce00114e

conformations. Instead, this suggests that subtle variations in intermolecular interactions within a fixed stoichiometric framework can result in distinct optical differences in co-crystals. This study provides new insights into the structural and optical properties of co-crystals, demonstrating how the interplay of π-hole···π and C–H···π interactions[30–32] and crystallization dynamics can lead to unique polymorphic behaviors. These findings not only expand the understanding of polymorphism in co-crystals but also pave the way for designing materials with tunable optical properties.

Compound **1** was prepared through a condensation reaction between 1,2-diphenylethane-1,2-dione and 5,6-diaminopyrazine-2,3-dicarbonitrile.[29] The compound was purified by column chromatography (silica gel, $CHCl_3$), yielding a pale yellow solid. While the crystal structure of this compound has already been reported, we became interested in the π-hole characteristics of the ten-membered ring framework of the pyrazinacene and attempted to co-crystallize it with naphthalene molecules. Naphthalene, a compound requiring proper regulation and management due to its status as an environmental pollutant,[33,34] has attracted attention for its molecular recognition behavior.[28a,35–40] Crystals containing naphthalene as a guest molecule have been reported as components in co-crystals and as guest molecules in host materials such as MOFs. According to a CSD search (ver. 2024.1.0), 295 entries contain crystals with naphthalene-inserted, among which approximately 70 examples for organic co-crystals. To the best of our knowledge, only one example of these entries exhibiting pseudo-polymorphism has been reported.[41] In contrast, we have previously reported the incorporation of naphthalene through electron-deficient metal centers designed using fluorinated ligands (M···π interactions)[28] and through donor–acceptor-type pyrazinacenes substituted with TPA (π-hole···π interactions).[42] These results prompted us to investigate the electron-donating effects of naphthalene. Typically, slow evaporation of **1** and an excess amount of **2** in a mixed solution of $CHCl_3$ and 2-propanol resulted in the formation of three distinct crystal forms: yellow prismatic crystals (**Y**) as the major product, red plate crystals (**R**) as the minor product, and colorless crystals of **2**. Initially, we assumed that the yellow crystals were single-component crystals of **1**, while the red crystals were co-crystals of **1** and **2**. However, thermogravimetric (TG) studies revealed that both crystals exhibited characteristic weight loss associated with the two-steps release of naphthalene, along with a shoulder observed around 90–105 °C for **Y** and 60–90 °C for **R**. Repeated experiments confirmed that both the yellow and red crystals encapsulate naphthalene (Fig. S1†).

The appearances and ORTEP views with numbering schemes of the prismatic and plate crystals, **Y** and **R**, respectively, at 160 K, are shown in Fig. 1, S2 and S3 and Table S1.† In **Y**, the asymmetric unit contains the full molecules of compounds **1** and **2**, confirming the 1 : 1 co-crystal composition (**1**·**2**). The pyrazinacene unit in **Y** is slightly twisted, with a dihedral angle of 3.51° between rings-

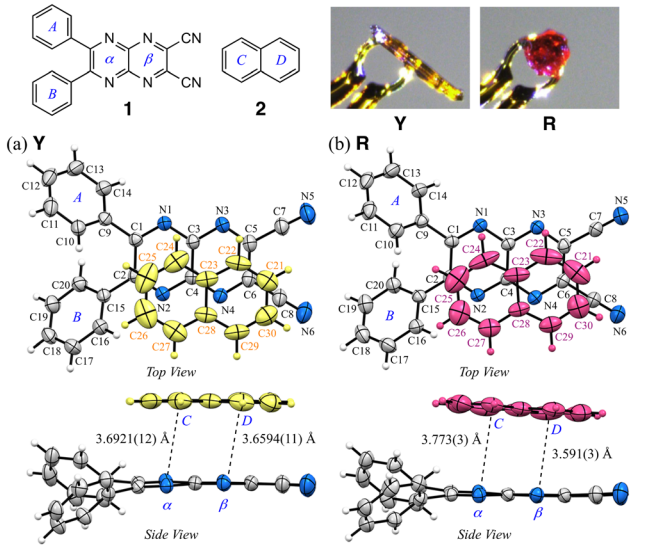

Fig. 1 The molecular structures in an asymmetric units of a) **Y** (CCDC 2419629) and b) **R** (CCDC 2419630) crystals at 160 K, showing the atom-labelling schemes. Displacement ellipsoids are drawn at the 50% probability level. The image on the top right shows the appearance of the resulting crystals. Color schemes: C, gray; N, blue; **2**, yellow and red.

α and β. Similarly, in **R**, the asymmetric unit also confirms the 1 : 1 co-crystal composition (**1**·**2**), with a dihedral angle of 3.33° between rings-α and β in the pyrazinacene unit. The puckering angles (τ) of the pyrazinacene moiety in **Y** and **R** are 2.6° and 2.1°, respectively, which are more twisted than those of the corresponding ten-membered rings in **2** (τ = 1.4° and 0.9° for **Y** and **R**, respectively). Molecular planarity also showed slight differences in the phenyl substituents, with the dihedral angles between pyrazinacene ring-α and phenyl groups, ring-*A* or ring-*B*, being slightly flatter in **R**: the angles for **Y** are 43.66° and 42.07°, while those for **R** are 40.88° and 41.24°. The intermolecular $C_g(\alpha\beta)\cdots C_g(CD)$ distances and dihedral angles between the ten-membered rings of the pyrazinacene moiety in **1** and the naphthalene core of **2** within the asymmetric unit reveal further distinctions. In **Y**, these values are 3.6758(10) Å and 1.58(6)°, with a slippage of 1.500 Å, along with a second naphthalene molecule positioned at 3.6086(10) Å, 1.58(6)°, and 1.082 Å. In **R**, the corresponding values are 3.682(3) Å, 5.27(9)°, and 1.241 Å, while the second naphthalene molecule is further apart at 5.289(3) Å. These observations suggest that π-hole···π interactions between the electron-deficient pyrazinacene core and the electron-rich naphthalene drive the formation of the co-crystals through three types of short aromatic stacking interactions. However, due to similar intramolecular conformations and stacking distances, these interactions alone do not fully explain the observed color differences. This raises intriguing questions about additional factors influencing the polymorphic behaviors, which are further explored in the analysis of packing structures.

The packing structures and the corresponding models of **Y** and **R** are shown in Fig. 2, where naphthalene molecules

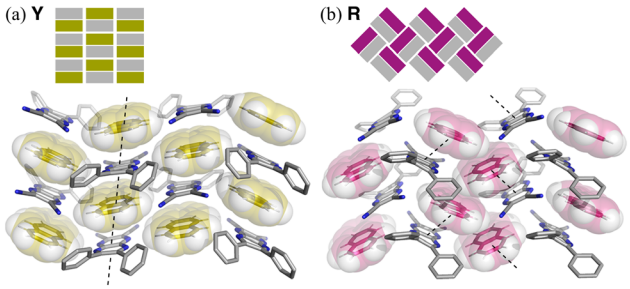

Fig. 2 Parts of each crystal packings of a) Y and b) R with schematic diagrams.

are represented in yellow and red, respectively, for clarity. Crystal **Y** features an alternating columnar arrangement of **1** and **2**, while crystal **R** exhibits paired **1** and **2** units arranged in a herringbone pattern. Reflecting this packing motif, **R** exhibits a higher density (D_c = 1.332 g cm^{-3}) compared to **Y** (D_c = 1.294 g cm^{-3}), which may influence their distinct optical properties. While single-component polymorphs often exhibit significant structural differences, such as variations in torsion angles or intramolecular bonding,[6–13] each molecular structure of **1** in **Y** and **R** of the co-crystal system remains unchanged. Therefore, we hypothesize that the difference in molecular packing density, with **R** adopting a more tightly packed arrangement, plays a key role in the observed color variation.

The detailed packing structure of **Y** is shown in Fig. 3. In the crystal, molecules **1** and **2** are alternately aligned along the *c*-axis through pseudo-hydrogen bonds and C–H···π interactions. The molecules are further alternately aligned in a columnar manner along the *b*-axis, forming π-hole···π

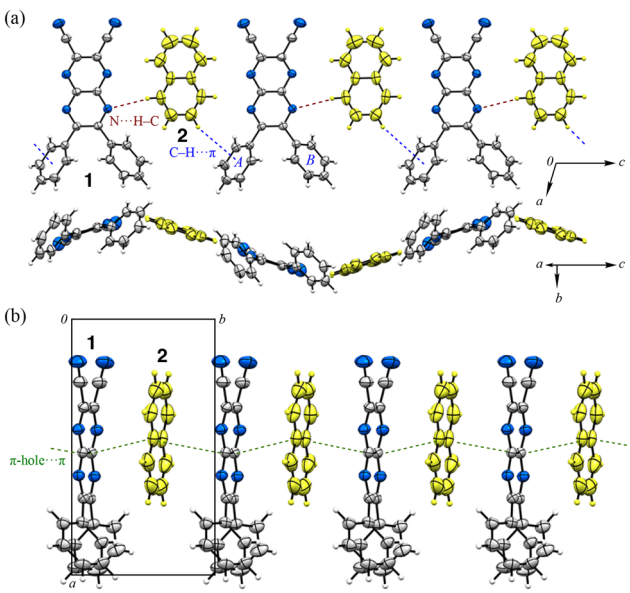

Fig. 3 a) Top (viewed along the *b*-axis) and side (rotated 90°) views of the packing structure with a layered arrangement, and b) columnar arrangement along the *b*-axis (viewed along the *c*-axis) of **Y**.

stacking interactions between **1** and **2** as well as between **2** and **1**^{i} (i: x, $y-1$, z). These parameters collectively underscore the role of π-interactions in stabilizing the crystal packing and suggest directional crystal growth.

In **R**, prominent C–H···π interactions are observed in the crystal (Fig. 4a). Notably, naphthalene rings are arranged in a zigzag pattern with minimal displacement between molecules along the *b*-axis (Fig. 4b). Specifically, interactions are observed for C27–H27···$C_g(D)$ and C29–H29···$C_g(C)$: the H···$C_g(D)$ distance for C27–H27···$C_g(D)$ is 2.96 Å, with C27···$C_g(D)$ at 3.752(4) Å, while the H···$C_g(C)$ distance for C29–H29···$C_g(C)$ is 2.85 Å, with C29···$C_g(C)$ at 3.642(4) Å. Additionally, the lone pairs on the nitrogen atoms in the pyrazinacene framework carry significant negative charge, which directs them toward electron-deficient regions on adjacent pyrazinacene planes: this arrangement forms a T-shaped configuration that is not observed in **Y**, with an intermolecular N3···$C_g(B)$ distance of 3.659 Å (Fig. 4c). From these observations, we hypothesize that the red crystal's structure is stabilized by treating the 1 : 1 combination of **1** and **2** as a single unit. This stability appears to be influenced by the preference for C–H···π interactions over π–π stacking, similar to the well-known preference of benzene in its most stable configurations.[43,44] The crystal of **1** without **2** also adopts a T-shaped configuration, where the lone pairs on the nitrogen atoms of the pyrazinacene point toward adjacent pyrazinacene planes. The shortest N···C_g(pyrazinacene) distance is 3.597 Å, while the corresponding distance on the opposite side is 4.047 Å. Consequently, when **R** is left standing for a few days at r.t., it gradually transforms into the yellow crystal *via* a crystal-to-crystal transition as **2** dissipates, yielding the crystal of **1**.

The Hirshfeld surface (HS) analysis was performed to quantify the contributions of intermolecular interactions on a per-atom basis,[45,46] and the resulting fingerprint plots and percentages are summarized in Table 1 and Fig. S4–S7.† In **Y**, stacking interactions between aromatic planes are prominent, while in **R**, edge-to-face interactions dominate, as clearly visualized in the plots. For the pyrazinacene framework of **1** in both crystals, the contribution of C···C

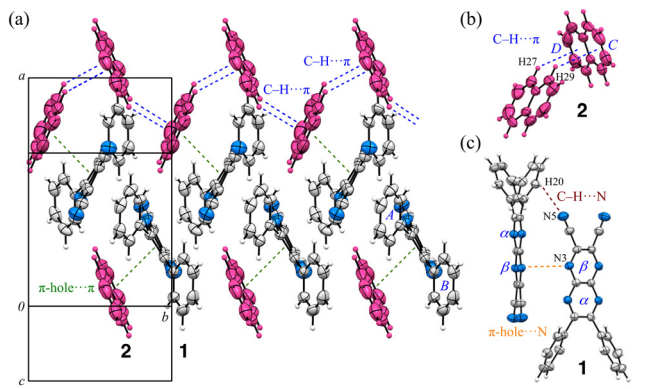

Fig. 4 (a) Part of the packing structure and the notable intermolecular interactions between (b) molecules **2** and (c) molecules **1** in crystal **R**.

Table 1 The intermolecular contribution of each atom calculated by HS analysis for each molecule in **Y** and **R** and reference data of the original crystal of **1** (ref. 29)

Crystal	**Y**		**R**		
Molecule	**1**	**2**	**1**	**2**	**1**
C···C	6.7	14.2	5.9	7.0	6.6
H···H	33.9	36.1	33.6	30.5	21.1
N···N	0.7	—	1.1	—	3.0
C···H/H···C	20.5	17.5	19.7	35.3	17.9
C···N/N···C	8.3	8.3	11.1	5.6	14.2
N···H/H···N	29.9	24.0	28.7	21.6	37.2

The isovalue is 0.002.

interactions is 6.7% in **Y** and 5.9% in **R**, showing only a slight difference. However, for the naphthalene molecules, these contributions are 14.2% in **Y** and 7.0% in **R**, indicating a significant twofold increase for **Y**. This result demonstrates that naphthalene in **Y** participates in π-hole···π stacking on both sides (*i.e.*, **2** is sandwiched by **1**), leading to closer face-to-face contacts compared to **R**, where stacking occurs on only one side. Similarly, the C···H/H···C contributions of naphthalene are much higher in **R** at 35.3%, compared to 17.5% in **Y**. This clearly highlights the stronger C–H···π interactions in **R**, as discussed earlier. While the π-hole···π interaction between the pyrazinacene framework and the π-system of naphthalene is common in both **Y** and **R**, the contributions of C···N/N···C interactions are higher in both **R** and the empty crystal of **1** compared to **Y**. This indicates that both **R** and the empty crystal adopt the T-shaped configuration.

To further understand the crystal color and additional properties, we investigated methods for selectively obtaining **Y** and **R**. According to our observations, dissolving **1** and **2** in an exact 1 : 1 molar ratio in $CHCl_3$ exclusively yielded red solids, indicating a preference for the formation of **R**. Mixing **1** with an excess amount of **2**, such as a tenfold molar ratio in a 1.5×10^{-2} mM solution, preferentially yielded yellow solids along with the independent precipitation of colorless crystals of **2**. This result suggests that, during crystallization, the kinetic formation of either a trimer (or a naphthalene-solvated environment) of **1** surrounded by **2** or a defined dimer (**1**·**2**) governs subsequent crystal growth (Scheme 2). With a slow crystallization process using 2-propanol, **Y** and **R** crystallized separately as a mixture. When naphthalene was limited, the solid adhered uniformly to the bottom of the test tube, whereas excess **2** caused the solids

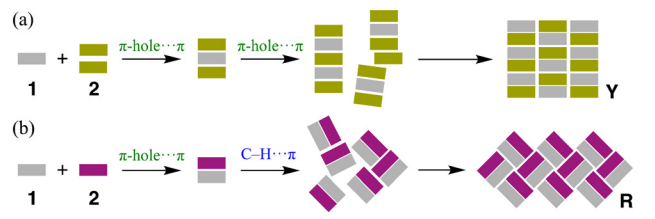

Scheme 2 Estimated co-crystallization processes of **1**·**2**: a) excess amount and b) the same stoichiometry of **2**.

to mix; however, these behaviors had no significant qualitative influence on the crystalline color. Solvent evaporation for high-quality crystal growth takes time (around two weeks), requiring a slight excess of **2** to prevent loss. However, under rapid precipitation conditions (on the order of hours), red solids could be kinetically synthesized. Conversely, when **R** was allowed to crystallize slowly, **Y** prismatic crystals were co-precipitated. Powder X-ray diffraction (pXRD) confirmed that the red and yellow solids obtained using this method corresponded to the single crystals of **Y** and **R**, respectively, while maintaining the original crystal structure of **2** (Fig. S8 and S9†).

Differential scanning calorimetry (DSC) analysis revealed that pure **1** remained stable up to 260 °C, while **2** exhibited an endothermic peak at 79.8 °C and melted at 81 °C. In contrast, the yellow solid showed a distinct endothermic peak at 81.3 °C, indicative of the presence of **2**, as well as a stepwise endothermic process around 100–110 °C. This additional peak suggests the incorporation of **2** into the **Y** crystal (Fig. 5a). The red solid, on the other hand, exhibits a broad endothermic peak starting at approximately 80 °C and reaching a maximum at 95.1 °C, corresponding to the desorption of **2**. Since no clear endothermic peaks corresponding to **2** and **Y** were observed separately from the broad peak of **R**, the presence of **2**, which TG and pXRD suggested to have been incorporated (Fig. S1†), could not be detected. However, the different thermal stabilities of **Y** and **R** confirm that they are distinct phases, even in their powdered states.

Solid-state absorption and emission spectra of the two solids were measured as shown in Fig. 5b and c, respectively. Pure **1** showed an absorption maximum at 430 nm with a shoulder at 460 nm and a weak emission band around 550 nm

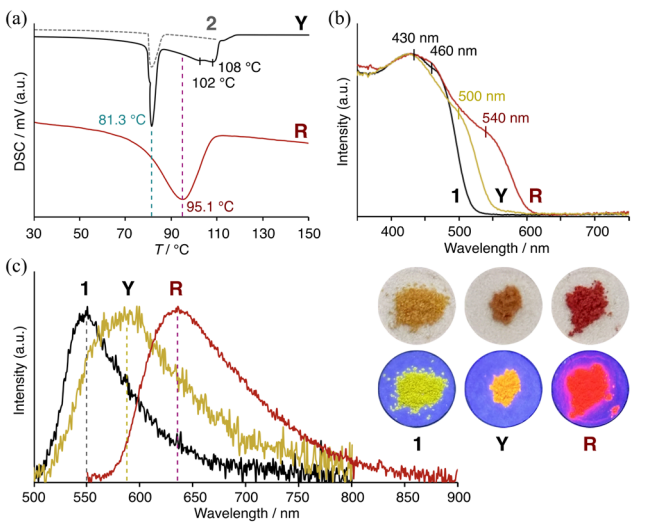

Fig. 5 a) DSC traces showing the thermal behavior of **Y**, **R**, and pure naphthalene (**2**) with increasing temperature. Solid-state b) absorption and c) emission spectra of **Y**, **R**, and the empty crystal of **1**. On the right, the top and bottom photos show the absorption colors under room light and the emission colors under UV irradiation (375 nm), respectively.

(λ_{ex} = 430 nm, PLQY = 0.6%). In contrast, **Y** containing naphthalene exhibited a slightly red-shifted shoulder absorption band around 500 nm and a weak emission band around 590 nm (λ_{ex} = 470 nm, PLQY = 1.0%). **R** also exhibited a red-shifted shoulder absorption around 540 nm (tailing up to 600 nm) and a remarkable emission band at 636 nm (λ_{ex} = 540 nm, PLQY = 11%), indicating both a red shift and higher emission intensity for **R** compared to **Y**. At this wavelength, the original solid of **2** mixed in as an impurity does not contribute to the emission properties. These results suggest that the formation of an exciplex between **1** and **2** as a unit through intermolecular interactions, and can be explained using the exciton model.[47–49] The additive transition moment of the two species in a dimer results in a lower transition energy for **R** compared to the individual compounds and **Y**. DFT calculations using the B3LYP 6-311+G(2df,2p)[50,51] and TDDFT B3LYP ma-def2-TZVP methods[52] for each compound, as well as for two units composed of four molecules (*i.e.*, parallel and T-shaped structures of **Y** and **R**, respectively), showed good agreement with the structural and photophysical stabilities (Fig. S10–S12†). Based on these results, the formation processes of the two different crystal systems support Scheme 2. When an excess of **2** is present, **1** becomes surrounded by **2**, and subsequent π-hole···π interactions lead to the formation of **Y**. In contrast, mixing **1** and **2** in a 1 : 1 ratio kinetically forms dimers, which serve as nuclei for the crystallization of **R** driven by C–H···π interactions. The resulting **R** crystal exhibits higher density, red-shifted absorption, and stronger red emission. This finding represents a significant departure from conventional structural mechanisms underlying polymorphic crystals with different colors. While changes in the mixing ratio are often associated with the formation of pseudo-polymorphic crystals, the formation of true polymorphs in a 1 : 1 co-crystal with distinct physical properties is a noteworthy advancement in crystal engineering.

In summary, the phenyl-substituted pyrazinacene (**1**) and naphthalene (**2**) co-crystals exhibited two distinct polymorphic forms, **Y** (yellow) and **R** (red), with unique structural and optical properties. Crystal **Y** demonstrated a columnar packing arrangement with π-hole···π stacking on both faces of naphthalene, while **R** adopted a herringbone motif with C–H···π interactions and a T-shaped configuration. Crystallographic and spectroscopic analyses revealed that **R** has a higher density, which correlates with the red-shifted absorption and stronger red-emission compared to **Y**, highlighting the critical role of intermolecular interactions in driving polymorphism. This study demonstrates how subtle variations in molecular arrangements influence the properties of co-crystals, providing insights into the supramolecular association process and intermolecular interactions with tailored optical and structural characteristics.

Data availability

The data supporting the findings of this study, including preparation methods, structural information, and physical properties, are available in the main article and its ESI.† Further inquiries regarding specific experimental details can be directed to the corresponding author.

Author contributions

K. N. prepared the samples, performed crystallographic, photophysical and theoretical investigations, and wrote original draft. G. J. R. provided support for the synthesis and theoretical investigations. A. H. supervised the project and wrote the manuscript. All authors contributed to discussions and to finalizing the manuscript.

Conflicts of interest

There are no conflicts to declare.

Acknowledgements

A. H. thanks Prof. Dr. Jun Yoshida of Nihon University for assistance with the DSC measurements. This work was supported by Grants-in-Aids for Scientific Research C, 24K08401 (G. J. R.) and Grant-in-Aids for Scientific Research B, 23K21122 (A. H.) of JSPS KAKENHI.

Notes and references

1 K. M. Steed and J. W. Steed, *Chem. Rev.*, 2015, **115**, 2895–2933, DOI: **10.1021/cr500564z**.
2 B. Moulton and M. J. Zaworotko, *Chem. Rev.*, 2001, **101**, 1629–1658, DOI: **10.1021/cr9900432**.
3 M. Irie, S. Kobatake and M. Horichi, *Science*, 2001, **291**, 1769–1772, DOI: **10.1126/science.291.5509.1769**.
4 R. H. Herber, M. Croft, M. J. Coyer, B. Bilash and A. Sahiner, *Inorg. Chem.*, 1994, **33**, 2422–2426, DOI: **10.1021/ic00089a018**.
5 R. S. Osborn and D. Rogers, *J. Chem. Soc., Dalton Trans.*, 1974, 1002–1004, DOI: **10.1039/DT9740001002**.
6 Y. Nishiuchi, A. Takayama, T. Suzuki and K. Shinozaki, *Eur. J. Inorg. Chem.*, 2011, 1815–1823, DOI: **10.1002/ejic.201001359**.
7 J. Fornies, S. Ibanez, A. Martin, M. Sanz, J. R. Berenguer, E. Lalinde and J. Torroba, *Organometallics*, 2006, **25**, 4331–4340, DOI: **10.1021/om0604526**.
8 J. S. Field, L. P. Ledwaba, O. Q. Munro and D. R. McMillin, *CrystEngComm*, 2008, **10**, 740–747, DOI: **10.1039/b717655d**.
9 R. I. Goldstein, R. Guo, C. Hughes, D. P. Maurer, T. R. Newhouse, T. J. Sisto, R. R. Conry, S. L. Price and D. M. Thamattoor, *CrystEngComm*, 2015, **17**, 4877–4882, DOI: **10.1039/C5CE00745C**.
10 M. Rubcic, K. Uzarevic, I. Halasz, N. Bregovic, M. Malis, I. Dilovic, Z. Kokan, R. S. Stein, R. E. Dinnebier and V. Tomisic, *Chem. – Eur. J.*, 2012, **18**, 5620–5631, DOI: **10.1002/chem.201103508**.
11 M. Louis, A. Brosseau, R. Guillot, F. Ito, C. Allain and R. Métivier, *J. Phys. Chem. C*, 2017, **121**, 15897–15907, DOI: **10.1021/acs.jpcc.7b01901**.

12 N. Oka, F. Ito, Y. Haketa, H. Maeda, T. Miyano, N. Tohnai, S. Ito, H. Miyasaka and S. Ozeki, *Chem. – Eur. J.*, 2018, **24**, 4343–4349, DOI: **10.1002/chem.201705356**.
13 G. Zhang, J. Lu, M. Sabat and C. L. Fraser, *J. Am. Chem. Soc.*, 2010, **132**, 2160–2162, DOI: **10.1021/ja9097719**.
14 C. Wang and Z. Li, *Mater. Chem. Front.*, 2017, **1**, 2174–2194, DOI: **10.1039/c7qm00201g**.
15 S. Kobatake, T. Yamada, K. Uchida, N. Kato and M. Irie, *J. Am. Chem. Soc.*, 1999, **121**, 2380–2386, DOI: **10.1021/ja983717j**.
16 R. A. van Delden, N. Koumura, N. Harada and B. L. Feringa, *Proc. Natl. Acad. Sci. U. S. A.*, 2002, **99**, 4945–4949, DOI: **10.1073/pnas.062660699**.
17 H. Zhang, Z. Zhang, K. Ye, J. Zhang and Y. Wang, *Adv. Mater.*, 2006, **18**, 2369–2372, DOI: **10.1002/adma.200600704**.
18 S. J. Yoon and S. Park, *J. Mater. Chem.*, 2011, **21**, 8338–8346, DOI: **10.1039/c0jm03711g**.
19 K. Ohno, H. Tanuma, Y. Kusano, S. Kaizaki, A. Nagasawa and T. Fujihara, *Dalton Trans.*, 2017, **46**, 7612–7618, DOI: **10.1039/c7dt00745k**.
20 S. J. Yoon, J. W. Chung, J. Gierschner, K. S. Kim, M. G. Choi, D. Kim and S. Y. Park, *J. Am. Chem. Soc.*, 2010, **132**, 13675–13683, DOI: **10.1021/ja1044665**.
21 B. R. Sreekanth, P. Vishweshwar and K. Vyas, *Chem. Commun.*, 2007, 2375–2377, DOI: **10.1039/b700082k**.
22 S. Aitipamula, P. S. Chowa and R. B. H. Tan, *CrystEngComm*, 2010, **12**, 3691–3697, DOI: **10.1039/c004491a**.
23 A. Lemmerer, D. A. Adsmond, C. Esterhuysen and J. Bernstein, *Cryst. Growth Des.*, 2013, **13**, 3935–3952, DOI: **10.1021/cg4006357**.
24 S. Aitipamula, P. S. Chowa and R. B. H. Tan, *CrystEngComm*, 2014, **16**, 3451–3465, DOI: **10.1039/c3ce42008f**.
25 J. H. Williams, *Crystal Engineering: How Molecules Build Solids*, Morgan & Claypool Publishers, 2017.
26 N. A. Mir, R. Dubey and G. R. Desiraju, *Acc. Chem. Res.*, 2019, **52**, 2210–2220, DOI: **10.1021/acs.accounts.9b00211**.
27 M. R. Ahsan, L. Singh, B. Sar and A. Mukherjee, *Cryst. Growth Des.*, 2024, **24**, 1695–1704, DOI: **10.1021/acs.cgd.3c01333**.
28 (*a*) Y. Ikumura, Y. Habuka, S. Sakai, T. Shinohara, H. Yuge, I. I. Rzeznicka and A. Hori, *Chem. – Eur. J.*, 2020, **26**, 5051–5060, DOI: **10.1002/chem.201905740**; (*b*) A. Hori, K. Nakajima and H. Yuge, *Acta Crystallogr., Sect. C: Struct. Chem.*, 2014, **70**, 960–964, DOI: **10.1107/S2053229614020294**.
29 G. J. Richards, J. P. Hill, N. K. Subbaiyan, F. D'Souza, P. A. Karr, M. R. J. Elsegood, S. J. Teat, T. Mori and K. Ariga, *J. Org. Chem.*, 2009, **74**, 8914–8923, DOI: **10.1021/jo901832n**.
30 S. W. Watt, C. Dai, A. J. Scott, J. M. Burke, R. Ll. Thomas, J. C. Collings, C. Viney, W. Clegg and T. B. Marder, *Angew. Chem., Int. Ed.*, 2004, **43**, 3061–3063, DOI: **10.1002/anie.200453828**.
31 A. Hori, A. Shinohe, M. Yamasaki, E. Nishibori, S. Aoyagi and M. Sakata, *Angew. Chem., Int. Ed.*, 2007, **46**, 7617–7620, DOI: **10.1002/anie.200702662**.
32 X. Pang, H. Wang, W. Wang and W. J. Jin, *Cryst. Growth Des.*, 2015, **15**, 4938–4945, DOI: **10.1021/acs.cgd.5b00844**.
33 P. S. Price and M. A. Jayjock, *Regul. Toxicol. Pharmacol.*, 2008, **51**, S15–S21, DOI: **10.1016/j.yrtph.2007.10.010**.
34 NTP, Toxicology and Carcinogenesis Studies of Naphthalene (CAS No 91-20-3) in F344/N Rats (Inhalation Studies) Technical Report Series No 500, National Toxicology Program, Research Triangle Park, NC, USA, 2000, pp. 1–173.
35 D. Liu, J. P. Lang and B. F. Abrahams, *J. Am. Chem. Soc.*, 2011, **133**, 11042–11045, DOI: **10.1021/ja203053y**.
36 V. I. Nikolayenko, A. Heynsa and L. J. Barbour, *Chem. Commun.*, 2017, **53**, 11306–11309, DOI: **10.1039/C7CC06676G**.
37 R. Liu, H. Wang and W. J. Jin, *Cryst. Growth Des.*, 2017, **17**, 3331–3337, DOI: **10.1021/acs.cgd.7b00299**.
38 J.-J. Liu, T. Liu, S.-B. Xia, C.-X. He, F.-X. Cheng, M.-J. Lin and C.-C. Huang, *Dyes Pigm.*, 2018, **149**, 59–64, DOI: **10.1016/j.dyepig.2017.09.058**.
39 S. Khatua and P. Biswas, *ACS Appl. Mater. Interfaces*, 2020, **12**, 22335–22346, DOI: **10.1021/acsami.0c02891**.
40 X. Wang, J. Zhao, M.-Q. Jia, X. D. Zhang, X. Xu, J. Cheng, Y. Wang, G.-X. Liu and K. Chen, *J. Solid State Chem.*, 2022, **316**, 123528, DOI: **10.1016/j.jssc.2022.123528**.
41 I. V. Fedyanin, *CrystEngComm*, 2022, **24**, 2591–2601, DOI: **10.1039/d2ce00081d**.
42 K. Nakada, G. J. Richards and A. Hori, *Chem. – Eur. J.*, 2025, e202404487, DOI: **10.1002/chem.202404487**.
43 A. Katrusiak, M. Podsiadło and A. Budzianowski, *Cryst. Growth Des.*, 2010, **10**, 3461–3465, DOI: **10.1021/cg1002594**.
44 E. Cox, *Nature*, 1928, **122**, 401, DOI: **10.1038/122401b0**; E. G. Cox, D. W. J. Cruickshank and J. A. S. Smith, *Proc. R. Soc. London, Ser. A*, 1958, **247**, 1–21, DOI: **10.1098/rspa.1958.0167**.
45 M. A. Spackman and D. Jayatilaka, *CrystEngComm*, 2009, **11**, 19–32, DOI: **10.1039/B818330A**.
46 M. J. Turner, J. J. McKinnon, S. K. Wolff, D. J. Grimwood, P. R. Spackman, D. Jayatilaka and M. A. Spackman, *CrystalExplorer*, vol. 17, 2017.
47 M. Kasha, *Radiat. Res.*, 1963, **20**, 55–70, DOI: **10.2307/3571331**.
48 K. Kumagai, M. Hasegawa, S. Enomoto and T. Hoshi, *Bull. Chem. Soc. Jpn.*, 2001, **74**, 441–447, DOI: **10.1246/bcsj.74.441**.
49 A. Hori, S. Takatani, T. K. Miyamotoa and M. Hasegawa, *CrystEngComm*, 2009, **11**, 567–569, DOI: **10.1039/B822007G**.
50 A. D. Becke, *J. Chem. Phys.*, 1993, **98**, 5648–5652, DOI: **10.1063/1.464913**.
51 C. Lee, W. Yang and R. G. Parr, *Phys. Rev. B*, 1988, **37**, 785–789, DOI: **10.1103/PhysRevB.37.785**.
52 F. Neese, *WIREs Comput. Mol. Sci.*, 2022, **12**, e1606.